ACS OMEGA

http://pubs.acs.org/journal/acsodf

Article

Proximal Methionine Amino Acid Residue Affects the Properties of Redox-Active Tryptophan in an Artificial Model Protein

Curtis A. Gibbs, Brooklyn P. Fedoretz-Maxwell,‡ Gregory A. MacNeil,‡ Charles J. Walsby, and Jeffrey J. Warren*

Cite This: *ACS Omega* 2023, 8, 19798−19806

Read Online

ACCESS | Metrics & More | Article Recommendations | Supporting Information

ABSTRACT: Redox-active amino acid residues are at the heart of biological electron-transfer reactions. They play important roles in natural protein functions and are implicated in disease states (e.g., oxidative-stress-associated disorders). Tryptophan (Trp) is one such redox-active amino acid residue, and it has long been known to serve a functional role in proteins. Broadly speaking, there is still much to learn about the local features that make some Trp redox active and others inactive. Herein, we describe a new protein model system where we investigate how a methionine (Met) residue proximal to a redox-active Trp affects its reactivity and spectroscopy. We use an artificial variant of azurin from *Pseudomonas aeruginosa* to produce these models. We employ a series of UV−visible spectroscopy, electrochemistry, electron paramagnetic resonance, and density functional theory experiments to demonstrate the effect that placing Met near Trp radicals has in the context of redox proteins. The introduction of Met proximal to Trp lowers its reduction potential by ca. 30 mV and causes clear shifts in the optical spectra of the corresponding radicals. While the effect may be small, it is significant enough to be a way for natural systems to tune Trp reactivity.

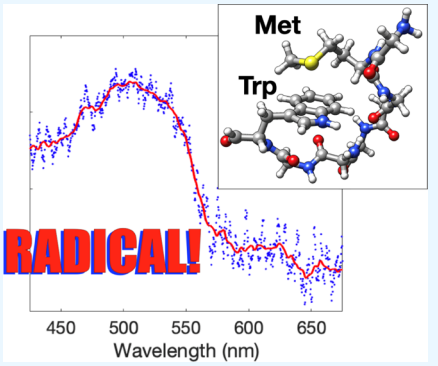

INTRODUCTION

Electron-transfer (ET) reactions involving amino acid residues are found in diverse biological systems.[1−4] There are many examples where redox cycling of amino acid residues is essential for functions (e.g., ribonucleotide reductases,[5] photosystem II,[6] cyclooxygenases[7]). Many examples involve reactions of tyrosine (Tyr) and tryptophan (Trp), but it should be noted that these are not the only redox-active residues. Redox-active amino acid residues can serve as either catalytic active sites or redox "waystations" in multistep ET chains.[1,2,8] Recent proposals have emerged where chains of Tyr and Trp residues can shuttle holes from embedded sites to protein surfaces where they can be quenched by endogenous reductants.[9−11] This establishes the broad importance of amino acid residue radicals, although there is still much to learn about how nature modifies proteins to support (or to impede) ET reactions.

The local structures (microenvironments) that house amino acids can substantially influence their reactivity.[3,12] Examples include the long-lived Tyr radical in Type II ribonucleotide reductase,[5,13] the hydrogen-bonded Tyr residue in photosystem II (Tyr_z),[6,14] and the hydrogen-bonded Trp indole in lignin/versatile peroxidases.[15,16] Herein, we are concerned with Trp and some examples of redox-active Trp and its microenvironments are shown in Figure 1.[17−19] Work from our research group,[20−22] and from others,[23−25] has shown that Trp amino acid residues are regularly found near Met in

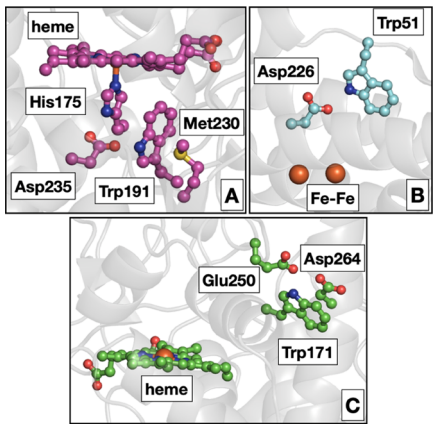

Figure 1. Examples of redox-active tryptophan (Trp) residues and other closely spaced amino acids (under 4 Å). Panel (A) shows yeast cytochrome *c* peroxidase (PDB ID 2CYP), panel (B) shows *Chlamydia trachomatis* ribonucleotide reductase (PDB ID 1SYY), and panel (C) shows *Phanerodontia chrysosporium* lignin peroxidase (PDB ID 1LLP).

Received: March 8, 2023
Accepted: May 11, 2023
Published: May 22, 2023

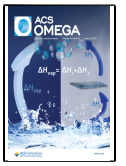

proteins from diverse organisms. There also are examples where the sites of Met−Trp interactions are redox active, with the best known example found in cytochrome *c* peroxidase.[26,27] These observations motivated the production and investigation of the protein models here, where Met is strategically introduced proximal to a redox-active Trp.

Despite the widespread distribution of Met−Trp interactions in biochemical systems and their roles in the protein structure,[24] there are still many knowledge gaps with respect to their roles in redox reactions. Small molecule model systems demonstrate that the interaction between a thioether and an aromatic group can confer unique reactivity and spectroscopy.[28,29] The unique properties of those systems were attributed to the formation of a two-center, three-electron bond in the oxidized molecules, which was supported and expanded upon in later theoretical work.[30,31] However, this type of bonding has not been clearly demonstrated in proteins. Other work on peptide models shows that the placement of Met between two aromatic redox sites can enhance long-range ET kinetics.[32,33] Interestingly, direct Met oxidation is unlikely and an interaction between Met and the peptide backbone can enhance ET. Thus, Met could facilitate ET even when not directly involved in redox chemistry.

The model systems described here are based on *Pseudomonas aeruginosa* azurin. Artificial variants of azurin have been widely used for the investigation of the spectroscopy and reactivity of Trp radicals housed in a biomolecule.[34−39] The discovery that a radical generated at Trp108[35] or at Trp48[36] in artificial azurin proteins was noteworthy; in particular, the long-lived Trp108 radical provides avenues to investigate its physical properties in detail.[34,35] In both of those cases, the radicals are readily generated using photochemistry[34,36,37] and the work described here builds upon these studies of the Trp108 radical. Here, we demonstrate how placement of a Met proximal to Trp108 alters its physical properties.

RESULTS

Design of Protein Model Systems. This work uses a known *P. aeruginosa* variant where all wild-type Tyr and Trp are replaced with phenylalanine (Phe) and the native histidine 83 (His83) is replaced with glutamine (Gln).[34,40,41] Specifically, the variations are Trp48Phe/Tyr72Phe/His83Gln/Tyr108Phe. This variant is known to be stable and have an intact Cu active site.[34,40,41] Additional mutations were added sequentially to give rise to the following amino acid variations: Gln107His, Phe108Trp, and Leu102Met. These additional amino acid substitutions yield the final models: Leu102-His107Trp108 and His107Trp108Met102. Each variant contains only one Trp residue, which substantially facilitates the below experiments where the physical properties of neutral Trp108 and the corresponding Trp108 radical are described.

Mutant azurins, Leu102His107Trp108 and Met102His107Trp108, were successfully expressed and purified. The identity and purity of the proteins were confirmed by UV−visible (UV−vis) spectrophotometry and mass spectrometry (Figure S2). The Cu(II)-cysteine112 (Cys112) charge-transfer band that imparts the blue color to azurin provides a convenient internal standard for optical spectroscopy (see the Supporting Information, Figure S1). Note that the Cu(II) site is at the opposite end of azurin than the Trp108 site so is unperturbed by the distant amino acid changes.

Absorbance and Fluorescence Properties of Trp108. The optical spectra of Leu102His107Trp108 and Met102His107Trp108 azurins show the expected $\pi-\pi^*$ transition band near 280 nm for Trp108 (Figure 2). Close inspection of

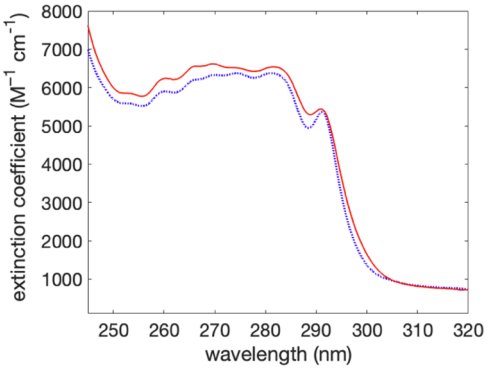

Figure 2. Optical spectra for Leu102His107Trp108 azurin (blue ●●●) and Met102His107Trp108 azurin (red −).

this $\pi-\pi^*$ transition band shows that no spectral shift is observed across the entire 240−300 nm range, suggesting that the energies of overlapping transitions to the ^1L_a and ^1L_b states[42] remain unchanged. The ^1L_a and ^1L_b states are the lowest energy electronic excited states of Trp that are responsible for its characteristic optical spectrum and those absorbance features can show a weak dependence on solvent dielectric.[43,44] There also are additional features observed at higher energies that are from the Phe residues present in the model protein.

Trp fluorescence is sensitive to changes in its microenvironment.[45] Both the excitation and the emission spectra of Leu102His107Trp108 and Met102His107Trp108 are shown in Figure 3. Similar to observations for the UV−vis spectra, the

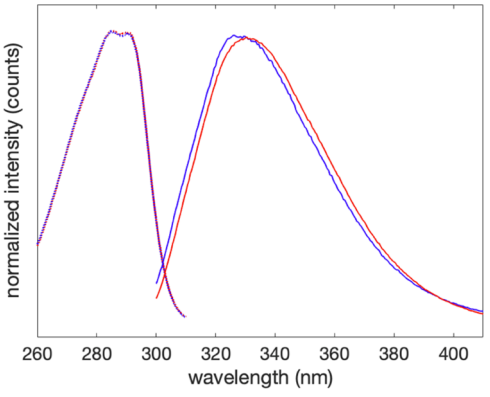

Figure 3. Excitation scans (λ_{em} = 350 nm, ●●●) for Leu102-His107Trp108 azurin (blue) and Met102His107Trp108 azurin (red) are shown on the left and emission scans (λ_{ex} = 270 nm, −) are shown on the right.

excitation spectra are superimposable. Interestingly, the emission spectra show changes with the amino acid substitution at position 102. This results in emission maxima at 328 and 331 nm for Leu102His107Trp108 and Met102His107Trp108, respectively. At the same concentrations, the emission intensity is the same for both proteins, indicating that no quenching of Trp fluorescence is induced by the presence of the Met102 residue.

https://doi.org/10.1021/acsomega.3c01589
ACS Omega 2023, 8, 19798−19806

Electrochemical Properties of Trp108. Cyclic voltammetry (CV) and differential pulse voltammetry (DPV) experiments were used to assess the potentials of the oxidation of Trp108. DPV features (Figure 4) are observed for

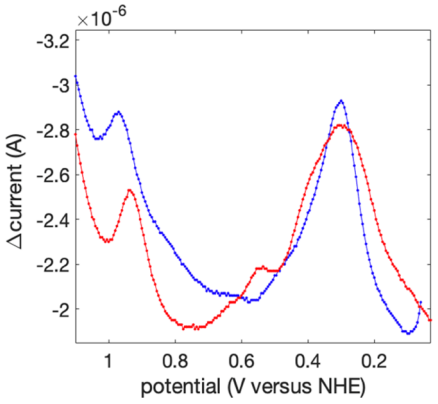

Figure 4. Differential pulse voltammogram for 70 μM Leu102-His107Trp108 azurin (blue) and 70 μM Met102His107Trp108 azurin (red). The apparent shoulders between 0.5 and 0.7 V are artifacts from the basal-plane graphite electrode material.

Leu102His107Trp108 at 0.30 V and at 0.97 V (potentials are reported versus the normal hydrogen electrode, NHE). The Trp108 radical reduction potential is similar to a recent report using a careful and systematic set of staircase voltammetry experiments.[39] The wave at 0.30 V is assigned to the Cu(II/I) redox couple.[46] For Met102His107Trp108, the waves are observed at 0.30 and 0.94 V. The same wave (0.30 V) is observed in the cyclic voltammograms (Supporting Information, Figure S3), in which Trp oxidation is a shoulder with only a weak return wave (i.e., mostly irreversible oxidation). There is, however, a weak inflection on the return scan, indicating a small degree of reversibility. This is consistent with the reported stability of Trp108 radicals. Note that we cannot discriminate between the one-electron and the one-electron + one-proton (i.e., proton-coupled) oxidation. Given the pH of the electrolyte (pH = 7.4), the proton-coupled oxidation is more likely. Note that electrode artifacts are observed at ca. 0.6 V in some DPV and CV experiments.

Absorbance Properties of the Trp108 Radical. The two azurin models were modified at His107 using [Re(I)-$(CO)_3$(4,7-dimethyl-1,10-phenanthroline)](CF_3SO_3) following the literature.[41,47] The labeled proteins show the expected UV−vis spectra for Re-modification (Figure S4). The Re(I) photosensitizer was chosen because of its known utility in generating Trp108 radicals in azurin.[34−36] For all UV−vis experiments involving Trp radicals, the samples were deoxygenated with repeated pump−N_2 purge cycles using a custom-made cuvette. The luminescence decay kinetics were monitored using time-resolved spectroscopy. The observed lifetimes (τ) of 125 ns ($k_{luminesence}$ = 8 × 10^6 s^{-1}) match literature reports (see Figure S5). No oxidation of Trp108 by the electronically excited *Re(I) is evident based on the decay kinetics. This is consistent with the excited-state potential for *Re(I) (i.e., *Re(I) to formally Re(0), 1.3 V vs NHE) and the above potentials determined for Trp108.

To generate Trp radicals, samples at a concentration of 57 μM were irradiated with 355 nm light for a frequency-tripled Nd:YAG laser (ca. 5 mJ per pulse) in the presence of the sacrificial electron acceptor $[Co(NH_3)_5Cl]Cl_2$ at 5 mM concentration. We note that this quencher has a low extinction coefficient and does not interfere with detection of Trp radicals in this work. The mechanism of Trp oxidation is likely via a formally Re(II) oxidant that is formed via quenching of electronically excited *Re(I) by $[Co(NH_3)_5Cl]Cl_2$. Preliminary UV−vis experiments showed that the Trp108 radical could be produced in Re(I)-modified Cu(II) azurins, but corresponding electron paramagnetic resonance (EPR) experiments were complicated by the presence of the paramagnetic Cu(II) ion in the azurin active site, which has a strong $g \sim 2$ component. As such, the corresponding Zn(II)-substituted proteins were prepared. Spectra were collected at different intervals to observe the formation of the Trp radical species and to determine a timepoint in which the Trp radical concentration maximizes (see the Supporting Information, Figure S6). Maximum yields were reached after about 45−60 s. Spectra of the Trp108 radical in both azurin models are set out in Figure 5. Both spectra were collected at 60 s for consistency.

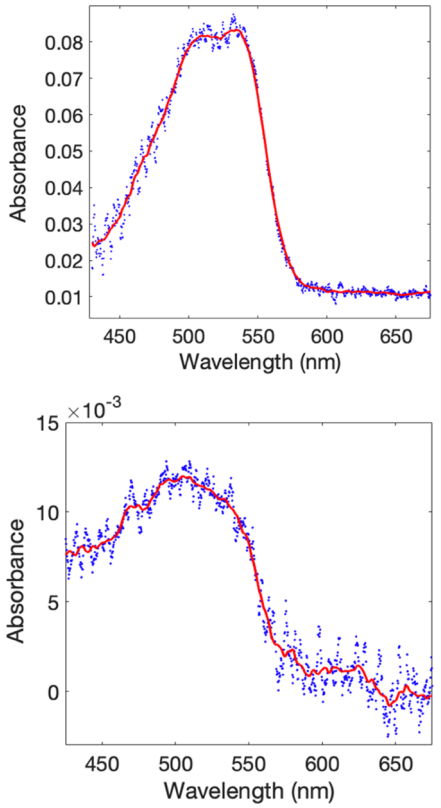

Figure 5. Optical spectra of Trp108 radicals in Leu102His107Trp108 azurin (top) and Met102His107Trp108 azurin (bottom). Spectra were generated using Re(I)-modified proteins, as described in the text. The blue dots show the experimental data, and the red line shows a moving average smoothed fit.

A comparison of the optical spectra of Trp108 radicals shows some important differences. First, the Trp108 radical in Leu102His107Trp108 azurin is readily produced, with λ_{max} centered at 522 nm. This is as described in the literature.[34−36] The corresponding Trp radical can be generated in Met102His107Trp108 azurin, but there is a clear difference in absorption intensity. There also is an apparent blue shift in the absorption maximum to $\lambda_{max} \sim 507$ nm, which may suggest some degree of deprotonation.[48] In general, the Trp radical in

https://doi.org/10.1021/acsomega.3c01589
ACS Omega 2023, 8, 19798−19806

Met102His107Trp108 azurin was less stable and the optical signals did not persist as long as those for Leu102-His107Trp108 azurin.

EPR Spectroscopy of Trp108 Radicals. To complement the steady-state UV−vis experiments outlined above, EPR was used to probe the electronic effects on the microenvironment surrounding the Trp108 radicals. In azurin, Trp radicals have been reported at position 48[36,37] and at position 108.[34,36,38] It is important to note that the Trp108 radical in Leu102-His107Trp108 azurin has been previously characterized[34,36,38] and was used as a benchmark for the experiments carried out here. Again, the Re(I)-labeled Zn(II) proteins were used and 5 mM $[ClCo(NH_3)_5]Cl_2$ was used as the sacrificial electron acceptor. As indicated above, the use of the Zn(II) proteins allows for a clearer analysis of Trp radical EPR by avoiding complications from overlapping signals for Cu(II).

The EPR spectra of Trp108 were collected for both Leu102His107Trp108 and Met102His107Trp108 using X-band EPR at 100 K. The spectra and their accompanying simulations are set out in Figure 6 and show the expected

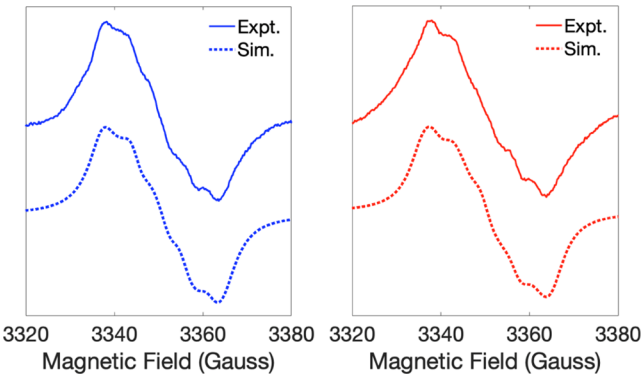

Figure 6. EPR spectra (100 K) for Leu102His107Trp108 azurin (blue, left panel) and Met102His107Trp108 azurin (red, right panel). The top spectra in each panel (solid lines) are experimental data and the bottom spectra (dotted lines) are the corresponding simulations.

shape with $g \sim 2$. The spectra for the Trp radical in Leu102His107Trp108 azurin are consistent with literature reports, including the g-values (Table 1).[34,36,38] The g-values reported here were obtained from EasySpin[49] simulations of the experimental spectra. The stated errors (Table 1) were estimated by manual variation of g and A values to establish the range of values that maintained the match between the simulated and experimental spectra. In all cases, the associated errors in g are within ±0.0002. The simulations for the Leu102His107Trp108 variant have slightly different g-values. Closer inspection of the EPR spectrum for both mutations reveals a hyperfine structure with hyperfine coupling constants (HFCCs) that are set out in the Supporting Information (Table S1). These values are consistent with the literature[34,36,38] and suggest that the spin density is primarily on the Trp ring, although the specific spin densities cannot be defined from these data. In addition, the EPR spectra for Met102His107Trp108 are consistent with reported spectra where there is some degree of deprotonation, or lack of hydrogen bonding, for a Trp radical.[38] The HFCCs we report produce EPR simulations that are consistent with our experiments and the g and A values are consistent with the literature.

Density Functional Theory (DFT) Calculations. DFT was used to provide further insights into the small changes to the UV−vis and EPR properties of Trp radicals in Leu102His107Trp108 and in Met102His107Trp108 azurins. Coordinates were taken from the literature (PDB ID: 1R1C) and a model was generated that contained Leu102 or Met102, Trp108, and the peptide backbone that connects amino acid residues 102−108. Side chains other than positions 102 and 108 were eliminated to lower computational cost. Six models were investigated (three for each protein): the closed hydrogen atoms were added programmatically and optimized (with all other atoms fixed) with the B3LYP functional and the Ahlrichs def2-SVP basis set. Next, the entire structure was optimized with the positions of the α-carbons fixed using the def2-TZVP basis set. All calculations included dispersion correction. The optimized structures are set out in Figure 7. A comparison to the experimental structure is shown in the Supporting Information (Figures S8 and S9).

The optimized structures of the radicals were used in time-dependent DFT (TD-DFT) calculations using the PBE0 functional and def2-TZVP basis set. B3LYP (and other functionals) can overestimate the energies of electronic transitions in biomolecules and PBE0 was shown to have improved performance in this regard.[51] The results from TD-DFT are shown in Figure 8. The solid lines show the predicted transitions for the Trp108 radical cations and the dashed lines show the neutral Trp108 radicals (i.e., deprotonated). The solid lines are reproduced from Figure 5, above. A full list of all transitions calculated and their relative intensities is given in the Supporting Information (Tables S2 and S3). Electron difference maps for the strongest transition also are shown (Figure S10). In addition to TD-DFT, EPR g-values were calculated for both the radical cation and neutral radicals for

Table 1. EPR g-Values for Trp108 Radicals[a]

	g_x	g_y	g_z	g_{iso}
Leu102Trp108[36]	2.00355	2.00271	2.00221	2.00282
Leu102Trp108[38]	2.00346	2.00264	2.00216	2.00275
Leu102Trp108 (exp)	2.0038(1)	2.0031(1)	2.0016(1)	2.0028(2)
Leu102Trp108$^{\bullet+}$ (calc)	2.00482	2.00391	2.00192	2.00355
Leu102Trp108$^{\bullet}$ (calc)	2.00379	2.00278	2.00148	2.00268
Met102Trp108 (exp)	2.0048(1)	2.0031(1)	2.0017(2)	2.0035(2)
Met102Trp108$^{\bullet+}$ (calc)	2.00603	2.00271	2.00171	2.00348
Met102Trp108$^{\bullet}$ (calc)	2.00382	2.00276	2.00122	2.00260

[a]In the cases of the calculated values, g-values for both the neutral radical (Trp108$^{\bullet}$) and the protonated radical cation (Trp108$^{\bullet+}$) are indicated as such.

https://doi.org/10.1021/acsomega.3c01589
ACS Omega 2023, 8, 19798−19806

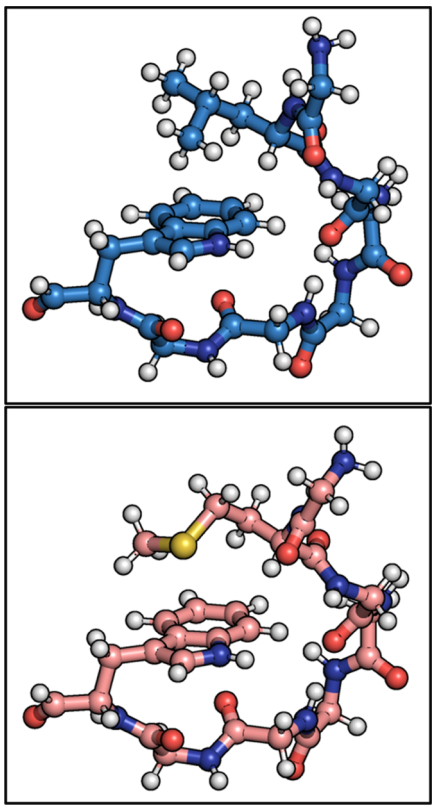

Figure 7. DFT-optimized structures for Leu102His107Trp108 azurin (blue, top panel) and Met102His107Trp108 azurin (pink, bottom panel). Structures shown are for the Trp108 radical cations. Images were generated using UCSF Chimera.[50]

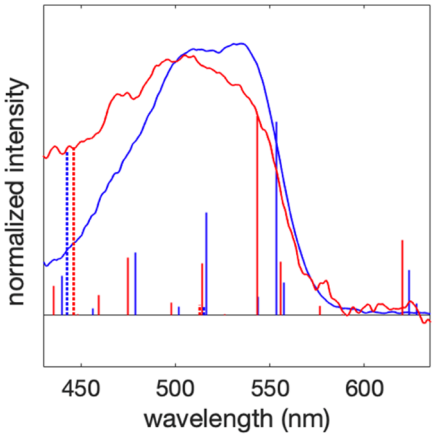

Figure 8. Comparison between TD-DFT (vertical lines) and experimental Trp108 radical UV−vis spectra. The solid lines are calculated transitions for Trp108 radical cations and the dashed lines are for neutral Trp108 radicals. Blue is for Leu102His107Trp108 azurin and red is for Met102His107Trp108 azurin.

Trp108 in Leu102His107Trp108 and Met102His107Trp108 azurins. The calculated *g*-values are set out in Table 1.

DISCUSSION

Trp radicals have important roles in biological systems, but there is still much to learn about how nature uses specific protein environments to control Trp reactivity. Here, we started with a known azurin system that can support a relatively long-lived Trp radical, that is, Leu102His107Trp108 azurin. Leu102 was substituted with Met and the corresponding proteins were investigated in both their closed-shell and radical forms. The optical spectra (Figure 2) of Trp108 are effectively the same in both protein systems. If any change were present, it would likely appear in the more broad portion of the spectrum, which corresponds to the ^1L_a band of Trp.[42] The excitation spectra (Figure 3) are similarly superimposable and show the expected emission primarily from absorption into the ^1L_a band. However, the Trp emission spectra show a small red shift for the Met102His107Trp108 protein, which could suggest a more polar (or solvent accessible) Trp site. So far, attempts to crystallize the Met102His107Trp108 protein have been unsuccessful, and such data would help to confirm the degree of solvent accessibility.

While the spectra of the closed-shell Trp108 sites are similar in Leu102His107Trp108 and Met102His107Trp108 azurins, some differences are observed for the radicals. First, the reduction potential for Trp108 radicals shifts by about 30 mV (0.97 V for Leu102His107Trp108 and 0.94 V). In the low driving force regime (0−200 meV), this would correspond to about a factor of two difference in electron-transfer rates, as calculated using common estimates of protein electron-transfer parameters using the semiclassical rate expression.[52−54] In addition, the optical spectra of the Trp108 radicals show differences. The Trp108 radical in Met102His107Trp108 azurin shows a blue shift to be ca. 10−15 nm (at the peak maxima). The optical spectrum for Trp108 in Leu102-His107Trp108 azurin is more consistent with the protonated radical (i.e., $Trp108^{\bullet+}$). The blue-shifted spectrum for Met102His107Trp108 azurin is suggestive of a more neutral radical character.[48] Likewise, the changes to the EPR spectra of Met102His107Trp108 with respect to Leu102His107Trp108 indicate changes to protonation or hydrogen bonding to Trp108.[38]

The DFT calculations offer an alternative viewpoint. The TD-DFT calculations for the fully protonated $Trp108^{\bullet+}$ predict a ca. 10 nm blue shift when Leu102 is replaced with Met102, consistent with experimental data. The TD-DFT transition calculations for neutral $Trp108^{\bullet}$ (dashed vertical lines in Figure 8) are not consistent with our experiments. The calculated EPR parameters are less conclusive, though the trend calculated for the cation radicals is in better agreement with the experimental data. Note also that hyperfine interactions were only computed for the protons and nitrogen associated with Trp. Overall, our truncated model calculated with implicit solvent (dielectric continuum) may obscure some of the more subtle hydrogen bonding and other noncovalent effects that can be important in the spectroscopy of Trp radicals.[38]

The largest observed changes are for the Trp108 reduction potential and the optical spectra of its radical. The 30 mV cathodic shift in potential for Trp oxidation in Met102His107Trp108 azurin is consistent with a more electron-rich site. Again, this can be due to the polarity of the proximal Met or from a somewhat great degree of solvent accessibility (see below). The blue shift in the optical spectra of the Trp108 radical in Met102His107Trp108 azurin could be due to a slightly greater amount of deprotonation. Assuming a Nernstian $E°/pK_a$ relation, 30 mV is about 0.5 pK_a units. Such a change may also be related to the lower apparent stability of Trp108 radicals in Met102His107Trp108 azurin. We note that the TD-DFT calculations suggest that the Trp radicals in both variants are mostly protonated.

https://doi.org/10.1021/acsomega.3c01589
ACS Omega 2023, 8, 19798−19806

Comparisons between azurin Trp108 radicals and other Trp radicals in azurin have been reported.[36−38] Trp108 is a partially solvent-exposed (ca. 40%) residue in azurin and in aqueous buffer, and Trp108 is already surrounded by a polar microenvironment dictated by the solvent. Hydrogen-bonding interactions have been identified using advanced EPR methods.[38] Our data does not suggest loss of structure in the Trp108 site, but the site is more polar (based on emission data). It is also suggested that a more polar microenvironment is responsible for a shift in Trp emission to a longer wavelength.[55] Therefore, a change to the weakly polar Met102 could include such a change to the Trp108 pocket or could increase solvent accessibility. In addition, the region surrounding Trp108 tends to be a slightly more disordered region of azurin, as evinced by structural β factors (e.g., in publicly available data sets from the PDB, including structure IDs: 4AZU, 1R1C, and 1E65).

CONCLUSIONS

Trp microenvironments have distinct impacts on their reactivity. Many Trp sites (Figure 1) have anionic residues in their local environments that may serve to stabilize Trp radical cations and maintain high levels of free energy (e.g., in the activation of lignin[19]). While it is widely known that Met can localize near Trp, its influence is not yet clear. Herein, we demonstrate that the placement of Met near Trp108 in azurin lowers the potential for Trp oxidation and affects its other physical properties (i.e., EPR and optical). The effect of replacing a Leu with a Met proximal to Trp108 produced biologically significant changes to Trp properties, in particular, in shifting reduction potentials. Further work is needed on these, and new, model systems to fully understand how nature specifically controls redox properties of Trp sites in proteins.

MATERIALS AND METHODS

General. All reagents were obtained from Sigma-Aldrich and used without further purification unless otherwise noted. Luria−Bertani (LB) broth miller was purchased from BioShop Canada and prepared according to the manufacturer. Water used was from a Barnstead EASYpure system (18 MΩ cm^{-1}). UV−vis spectrophotometry was carried out using a Cary 100-Bio spectrophotometer. MALDI mass spectrometry was carried out on a Bruker microflex LT MALDI Biotyper mass spectrometer. Transient absorption experiments were carried out using a home-built spectrometer containing an Continuum Surelite SLI-10 (Nd:YAG) laser, a Continuum Surelite OPO, a 75 W Xe arc lamp, and a home-built detection system. Full details of the system are described elsewhere.[56] Steady-state UV−vis experiments were carried out using the same home-built laser system but with a Photon Control detector and deuterium−halogen light source. Electrochemistry experiments were carried out using a CH Instruments 6171B potentiostat.

Plasmid Construction. The "all-Phe" azurin plasmid (i.e., all native Trp and Tyr replaced with Phe) was a gift from H. B. Gray and J. H. Richards (California Institute of Technology). The Phe108Trp mutation was added followed by Leu102Met so that two distinct protein scaffolds could be expressed (Leu102His107Trp108 and Met102His107Trp108). All mutations were introduced using standard site-directed protocols.[57] DNA primers were purchased from Eurofins Genomics. Q5 DNA polymerase and *Dpn*I enzyme were purchased from New England BioLabs (NEB). Plasmids were sequenced by Eurofins Genomics.

Protein Expression and Purification. Plasmids were transformed into competent BL21(DE3) *Escherichia coli* cells grown on ampicillin-containing agar plates. Single colonies were selected for liquid starter cultures in LB broth containing 100 μg mL^{-1} ampicillin. Starter cultures were grown at 37 °C with shaking at 180 rpm for 6 h. Overnight expression cultures were prepared by adding 3 mL of starter culture into LB broth with 100 μg mL^{-1} ampicillin and 0.4% glycerol as a glassing agent. Overnight expression cultures were grown at 37 °C with shaking at 180 rpm. Cells were then pelleted by centrifugation at 4000 rpm. Cell pellets were resuspended in osmotic shock buffer (50 mM Tris, 1 mM EDTA, 20% sucrose, pH 8.1) and rested on ice for 20 min. Cell pellets were then obtained by centrifugation at 7000 rpm. Pellets were resuspended in 500 μM $MgCl_2$ and rested on ice for 20 min. Proteins were isolated by centrifugation at 12000 rpm. The resulting supernatant fractions were collected and 100 mM $CuSO_4$ and 500 mM NaOAc (pH 4.5) were added dropwise to final concentrations of 1 and 5 mM, respectively. These mixtures were incubated overnight at 37 °C to promote Cu(II) uptake by apo-azurin. Acid-precipitated proteins were removed by centrifugation at 12000 rpm. The resulting supernatants were collected and purified on a CM Sepharose column obtained from GE Healthcare using a NaOAc concentration gradient. Protein purities and concentrations were determined spectrophotometrically using reported extinction coefficients (ε_{628} = 5600 M^{-1} cm^{-1}).[56,58]

Preparation of Zn(II)-Substituted Azurins. Protein samples were desalted into 10 mM NaOAc at pH 7.5 before a minimal addition of stripping solution (100 mM NaOAc, 1 mM EDTA, and 100 mM NaCN at pH 9) dropwise with constant agitation. This is done until a colorless solution of azurin is observed. Proteins were exchanged into 10 mM NaOAc at pH 7.5 to remove NaCN. A 6 mL aliquot of 100 mM $Zn(OAc)_2$ (6 mL) was added to both protein samples and shaken at 180 rpm at 37 °C overnight. A white precipitate is formed overnight and spun down at 3000 rpm. The resulting colorless samples were decanted and further concentrated before being stored at 4 °C.

Modification with Triflato-Re(I)(4,7-dimethylphenanthroline)tricarbonyl ($Re(CO)_3$(4,7-dmp)OTf). Labeled azurins were obtained by adding 2 equiv of [$Re(CO)_3$(4,7-dmp)OTf] to a solution of azurin in 25 mM HEPES (pH 7.0). These reaction mixtures were incubated for 5−7 days at 37 °C in the dark. The reaction vessel was spun down at 3000 rpm to remove any precipitates. FPLC was carried out using a HiTrap IMAC FF column (obtained from GE Healthcare) that was activated with Cu^{2+}. The reaction mixture was then exchanged into binding buffer (1 M NaCl, 20 mM NaPi, pH 7.8) and loaded to the previously equilibrated column under the same buffer system. Unmodified azurins bound to the column while Re-modified azurins (Re-Leu102His107Trp108 and Re-Met102His107Trp108) elute with the binding buffer wash. Unlabeled azurins were collected and pooled for reuse. Rhenium(I)-modified fractions were collected and monitored by UV−vis spectrophotometry to pool correct fractions together. Concentrations of each Re-modified azurin were calculated spectrophotometrically using reported extinction coefficients.[47]

Tryptophan Fluorescence Measurements. Fluorescence experiments were carried out using a Horiba Jobin-

https://doi.org/10.1021/acsomega.3c01589
ACS Omega 2023, 8, 19798−19806

Yvon Fluorolog. Samples (60 μM protein) were prepared in 1 M NH_4Cl and 20 mM NaP_i at pH 7.8. Samples were placed into air-free cuvettes made by the Simon Fraser University (SFU) Glass Shop and deoxygenated with 15−20 pump-backfill cycles using N_2. Excitation was achieved using 280 nm light, and spectra were recorded from 295 to 500 nm to monitor for Trp fluorescence. 10 scans were performed per sample and emission maxima were determined by averaging each series.

Electrochemical Measurements. A standard three electrode setup was used with a basal-plane graphite working electrode, a platinum counter electrode, and a AgCl/Ag reference electrode. Protein samples (70 μM) were prepared in 0.1 M sodium acetate, pH 5. Cyclic voltammetry scans were collected at a scan rate of 20 mV per second. DPV experiments used a 5 mV increment, 50 mV pulse amplitude, 50 ms pulse width, and 10 ms sample period.

EPR Measurements. Protein samples (200 μL, 30−100 μM) were prepared in 50 mM NaP_i at pH 7.5 with 30% glycerol and 5 mM $[Co(NH_3)Cl]Cl_2$ as an electron acceptor. Pump-backfill cycles (15−20 total) using N_2 were performed to remove O_2 from the sample. Samples were immediately transferred into EPR tubes and irradiated with defocused 355 nm pulses from a frequency-tripled Nd:YAG laser (7 ns pulse width, 8−10 mJ $pulse^{-1}$). Immediately following irradiation, samples were flash frozen and stored in liquid N_2 before EPR experiments. EPR experiment was carried out using a Bruker EMXplus spectrometer using an X-band Premium X microwave and HS resonator. Experiments were carried out at 100 K using a Bruker ER 4112HV temperature controller with a continuous flow cryostat using liquid N_2. Typical operation parameters were as follows: microwave frequency, 9.39 GHz; microwave power, 2 mW; and modulation amplitude, 5 Gauss. Measurement of solid 2,2-diphenyl-1-picrylhydrazyl (DPPH) was used as a calibration standard (g = 2.0036(2)).[59] EPR simulations were carried out using EasySpin software.[49]

Density Functional Theory Calculations. Calculations were performed using the ORCA 5.0.3 ab initio quantum chemistry program.[60−62] Geometry optimizations and single point calculations were carried out using the B3LYP functional, utilizing the RIJCOSX algorithm.[63] The Becke−Johnson damping scheme was used in all calculations.[64,65] All calculations accounted for water solvent using a dielectric continuum model (CPCM).[66] Protein models were generated from publicly available X-ray coordinates (PDB ID: 1R1C). Amino acid side chains were removed and hydrogen atoms were added programmatically in PyMOL. Hydrogen positions were optimized with heavy atom positions fixed using the def2-SVP/def2/J basis set.[67,68] Next, all atoms were optimized with the positions of the α-carbon positions fixed using the def2-TZVP basis set. TD-DFT calculations were carried out using the PBE0 functional[69,70] and def2-TZVP basis set. EPR g-values were calculated using the B3LYP functional and def2-SVP basis set.

■ ASSOCIATED CONTENT

Supporting Information

The Supporting Information is available free of charge at https://pubs.acs.org/doi/10.1021/acsomega.3c01589.

Full optical spectra for azurins and Re(I)-azurins; mass spectrometry data for Leu102His107Trp108 azurin; cyclic voltammograms of azurins; time-resolved luminescence traces of Re-modified azurins; additional protein structures; TD-DFT electron density maps for Trp cation radical transitions; and tabulated TD-DFT transition energies (PDF)

■ AUTHOR INFORMATION

Corresponding Author

Jeffrey J. Warren − *Department of Chemistry, Simon Fraser University, Burnaby, British Columbia V5A 1S6, Canada;* orcid.org/0000-0002-1747-3029; Email: jjwarren@sfu.ca

Authors

Curtis A. Gibbs − *Department of Chemistry, Simon Fraser University, Burnaby, British Columbia V5A 1S6, Canada*

Brooklyn P. Fedoretz-Maxwell − *Department of Chemistry, Simon Fraser University, Burnaby, British Columbia V5A 1S6, Canada*

Gregory A. MacNeil − *Department of Chemistry, Simon Fraser University, Burnaby, British Columbia V5A 1S6, Canada*

Charles J. Walsby − *Department of Chemistry, Simon Fraser University, Burnaby, British Columbia V5A 1S6, Canada;* orcid.org/0000-0003-3194-8227

Complete contact information is available at: https://pubs.acs.org/10.1021/acsomega.3c01589

Author Contributions

‡B.P.F.M. and G.A.M. contributed equally and are listed in alphabetical order. The manuscript was written through contributions of all authors. All authors have given approval to the final version of the manuscript.

Notes

The authors declare no competing financial interest.

■ ACKNOWLEDGMENTS

Financial support from the Natural Sciences and Engineering Research Council of Canada (NSERC, Discovery Grant Program, RGPIN-06272 to J.J.W.) and Simon Fraser University supported this work. The computational efforts here were enabled by support provided by the Digital Research Alliance of Canada (alliancecan.ca).

■ REFERENCES

(1) Stubbe, J.; van der Donk, W. A. Protein Radicals in Enzyme Catalysis. *Chem. Rev.* **1998**, *98*, 705−762.

(2) Stubbe, J.; Nocera, D. G. Radicals in Biology: Your Life Is in Their Hands. *J. Am. Chem. Soc.* **2021**, *143*, 13463−13472.

(3) Tommos, C. Insights into the Thermodynamics and Kinetics of Amino-Acid Radicals in Proteins. *Ann. Rev. Biophys.* **2022**, *51*, 453−471.

(4) Winkler, J. R.; Gray Harry, B. Could Tyrosine and Tryptophan Serve Multiple Roles in Biological Redox Processes? *Philos. Trans. R. Soc., A* **2015**, *373*, No. 20140178.

(5) Kang, G.; Taguchi, A. T.; Stubbe, J.; Drennan, C. L. Structure of a Trapped Radical Transfer Pathway within a Ribonucleotide Reductase Holocomplex. *Science* **2020**, *368*, 424−427.

(6) Lubitz, W.; Chrysina, M.; Cox, N. Water Oxidation in Photosystem II. *Photosynth. Res.* **2019**, *142*, 105−125.

(7) Liu, Y.; Roth, J. P. A Revised Mechanism for Human Cyclooxygenase-2. *J. Biol. Chem.* **2016**, *291*, 948−958.

(8) Warren, J. J.; Ener, M. E.; Vlček, A.; Winkler, J. R.; Gray, H. B. Electron Hopping through Proteins. *Coord. Chem. Rev.* **2012**, *256*, 2478−2487.

(9) Winkler, J. R.; Gray, H. B. Electron Flow through Biological Molecules: Does Hole Hopping Protect Proteins from Oxidative Damage? *Q. Rev. Biophys.* **2015**, *48*, 411−420.
(10) Polizzi, N. F.; Migliore, A.; Therien, M. J.; Beratan, D. N. Defusing Redox Bombs? *Proc. Natl. Acad. Sci. U.S.A.* **2015**, *112*, 10821−10822.
(11) Gray, H. B.; Winkler, J. R. Hole Hopping through Tyrosine/Tryptophan Chains Protects Proteins from Oxidative Damage. *Proc. Natl. Acad. Sci. U.S.A.* **2015**, *112*, 10920−10925.
(12) Westerlund, K.; Berry, B. W.; Privett, H. K.; Tommos, C. Exploring Amino-Acid Radical Chemistry: Protein Engineering and de Novo Design. *Biochim. Biophys. Acta, Bioenerg.* **2005**, *1707*, 103−116.
(13) Stubbe, J. Di-Iron-Tyrosyl Radical Ribonucleotide Reductases. *Curr. Opin. Chem. Biol.* **2003**, *7*, 183−188.
(14) Saito, K.; Shen, J.-R.; Ishida, T.; Ishikita, H. Short Hydrogen Bond between Redox-Active Tyrosine YZ and D1-His190 in the Photosystem II Crystal Structure. *Biochemistry* **2011**, *50*, 9836−9844.
(15) Pogni, R.; Baratto, M. C.; Teutloff, C.; Giansanti, S.; Ruiz-Dueñas, F. J.; Choinowski, T.; Piontek, K.; Martínez, A. T.; Lendzian, F.; Basosi, R. A Tryptophan Neutral Radical in the Oxidized State of Versatile Peroxidase from Pleurotus Eryngii. *J. Biol. Chem.* **2006**, *281*, 9517−9526.
(16) Ruiz-Dueñas, F. J.; Pogni, R.; Morales, M.; Giansanti, S.; Mate, M. J.; Romero, A.; Martinez, M. J.; Basosi, R.; Martinez, A. T. Protein Radicals in Fungal Versatile Peroxidase. *J. Biol. Chem.* **2009**, *284*, 7986−7994.
(17) Finzel, B. C.; Poulos, T. L.; Kraut, J. Crystal Structure of Yeast Cytochrome c Peroxidase Refined at 1.7-A Resolution. *J. Biol. Chem.* **1984**, *259*, 13027−13036.
(18) Högbom, M.; Stenmark, P.; Voevodskaya, N.; McClarty, G.; Gräslund, A.; Nordlund, P. The Radical Site in Chlamydial Ribonucleotide Reductase Defines a New R2 Subclass. *Science* **2004**, *305*, 245−248.
(19) Blodig, W.; Smith, A. T.; Doyle, W. A.; Piontek, K. Crystal Structures of Pristine and Oxidatively Processed Lignin Peroxidase Expressed in Escherichia Coli and of the W171F Variant That Eliminates the Redox Active Tryptophan 171. Implications for the Reaction Mechanism. *J. Mol. Biol.* **2001**, *305*, 851−861.
(20) Weber, D. S.; Warren, J. J. A Survey of Methionine-Aromatic Interaction Geometries in the Oxidoreductase Class of Enzymes: What Could Met-Aromatic Interactions Be Doing near Metal Sites? *J. Inorg. Biochem.* **2018**, *186*, 34−41.
(21) Weber, D. S.; Warren, J. J. The Interaction between Methionine and Two Aromatic Amino Acids Is an Abundant and Multifunctional Motif in Proteins. *Arch. Biochem. Biophys.* **2019**, *672*, No. 108053.
(22) Gibbs, C. A.; Weber, D. S.; Warren, J. J. Clustering of Aromatic Amino Acid Residues around Methionine in Proteins. *Biomolecules* **2022**, *12*, No. 6.
(23) Reid, K. S. C.; Lindley, P. F.; Thornton, J. M. Sulphur-aromatic Interactions in Proteins. *FEBS Lett.* **1985**, *190*, 209−213.
(24) Valley, C. C.; Cembran, A.; Perlmutter, J. D.; Lewis, A. K.; Labello, N. P.; Gao, J.; Sachs, J. N. The Methionine-Aromatic Motif Plays a Unique Role in Stabilizing Protein Structure. *J. Biol. Chem.* **2012**, *287*, 34979−34991.
(25) Aledo, J. C.; Cantón, F. R.; Veredas, F. J. Sulphur Atoms from Methionines Interacting with Aromatic Residues Are Less Prone to Oxidation. *Sci. Rep.* **2015**, *5*, No. 16955.
(26) Sivaraja, M.; Goodin, D. B.; Smith, M.; Hoffman, B. M. Identification by ENDOR of Trp191 as the Free-Radical Site in Cytochrome c Peroxidase Compound ES. *Science* **1989**, *245*, 738−740.
(27) Barrows, T. P.; Bhaskar, B.; Poulos, T. L. Electrostatic Control of the Tryptophan Radical in Cytochrome c Peroxidase. *Biochemistry* **2004**, *43*, 8826−8834.
(28) Chung, W. J.; Ammam, M.; Gruhn, N. E.; Nichol, G. S.; Singh, W. P.; Wilson, G. S.; Glass, R. S. Interactions of Arenes and Thioethers Resulting in Facilitated Oxidation. *Org. Lett.* **2009**, *11*, 397−400.
(29) Monney, N. P.-A.; Bally, T.; Bhagavathy, G. S.; Glass, R. S. Spectroscopic Evidence for a New Type of Bonding between a Thioether Radical Cation and a Phenyl Group. *Org. Lett.* **2013**, *15*, 4932−4935.
(30) Hendon, C. H.; Carbery, D. R.; Walsh, A. Three-Electron Two-Centred Bonds and the Stabilisation of Cationic Sulfur Radicals. *Chem. Sci.* **2014**, *5*, 1390−1395.
(31) Orabi, E. A.; English, A. M. Modeling Protein S−Aromatic Motifs Reveals Their Structural and Redox Flexibility. *J. Phys. Chem. B* **2018**, *122*, 3760−3770.
(32) Wang, M.; Gao, J.; Müller, P.; Giese, B. Electron Transfer in Peptides with Cysteine and Methionine as Relay Amino Acids. *Angew. Chem., Int. Ed.* **2009**, *48*, 4232−4234.
(33) Giese, B.; Wang, M.; Gao, J.; Stoltz, M.; Müller, P.; Graber, M. Electron Relay Race in Peptides. *J. Org. Chem.* **2009**, *74*, 3621−3625.
(34) Miller, J. E.; Grădinaru, C.; Crane, B. R.; Di Bilio, A. J.; Wehbi, W. A.; Un, S.; Winkler, J. R.; Gray, H. B. Spectroscopy and Reactivity of a Photogenerated Tryptophan Radical in a Structurally Defined Protein Environment. *J. Am. Chem. Soc.* **2003**, *125*, 14220−14221.
(35) Di Bilio, A. J.; Crane, B. R.; Wehbi, W. A.; Kiser, C. N.; Abu-Omar, M. M.; Carlos, R. M.; Richards, J. H.; Winkler, J. R.; Gray, H. B. Properties of Photogenerated Tryptophan and Tyrosyl Radicals in Structurally Characterized Proteins Containing Rhenium(I) Tricarbonyl Diimines. *J. Am. Chem. Soc.* **2001**, *123*, 3181−3182.
(36) Shafaat, H. S.; Leigh, B. S.; Tauber, M. J.; Kim, J. E. Spectroscopic Comparison of Photogenerated Tryptophan Radicals in Azurin: Effects of Local Environment and Structure. *J. Am. Chem. Soc.* **2010**, *132*, 9030−9039.
(37) Larson, B. C.; Pomponio, J. R.; Shafaat, H. S.; Kim, R. H.; Leigh, B. S.; Tauber, M. J.; Kim, J. E. Photogeneration and Quenching of Tryptophan Radical in Azurin. *J. Phys. Chem. B* **2015**, *119*, 9438−9449.
(38) Stoll, S.; Shafaat, H. S.; Krzystek, J.; Ozarowski, A.; Tauber, M. J.; Kim, J. E.; Britt, R. D. Hydrogen Bonding of Tryptophan Radicals Revealed by EPR at 700 GHz. *J. Am. Chem. Soc.* **2011**, *133*, 18098−18101.
(39) Tyson, K. J.; Davis, A. N.; Norris, J. L.; Bartolotti, L. J.; Hvastkovs, E. G.; Offenbacher, A. R. Impact of Local Electrostatics on the Redox Properties of Tryptophan Radicals in Azurin: Implications for Redox-Active Tryptophans in Proton-Coupled Electron Transfer. *J. Phys. Chem. Lett.* **2020**, *11*, 2408−2413.
(40) Shih, C.; Museth, A. K.; Abrahamsson, M.; Blanco-Rodriguez, A. M.; Di Bilio, A. J.; Sudhamsu, J.; Crane, B. R.; Ronayne, K. L.; Towrie, M.; Vlcek, A.; Richards, J. H.; Winkler, J. R.; Gray, H. B. Tryptophan-Accelerated Electron Flow Through Proteins. *Science* **2008**, *320*, 1760−1762.
(41) Miller, J. E.; Di, B.; Wehbi, W. A.; Green, M. T.; Museth, A. K.; Richards, J. R.; Winkler, J. R.; Gray, H. B. Electron Tunneling in Rhenium-Modified Pseudomonas Aeruginosa Azurins. *Biochim. Biophys. Acta, Bioenerg.* **2004**, *1655*, 59−63.
(42) Callis, P. R. [7] 1La and 1Lb Transitions of Tryptophan: Applications of Theory and Experimental Observations to Fluorescence of Proteins. In *Flourescence Spectroscopy*, Methods in Enzymology; Academic Press, 1997; Vol. *278*, pp 113−150.
(43) Strickland, E. H.; Billups, C.; Kay, E. Effects of Hydrogen Bonding and Solvents upon the Tryptophanyl 1La Absorption Band. Studies Using 2,3-Dimethylindole. *Biochemistry* **1972**, *11*, 3657−3662.
(44) Middendorf, T. R.; Aldrich, R. W.; Baylor, D. A. Modification of Cyclic Nucleotide−Gated Ion Channels by Ultraviolet Light. *J. Gen. Physiol.* **2000**, *116*, 227−252.
(45) Biswal, H. S.; Wategaonkar, S. Nature of the N−H···S Hydrogen Bond. *J. Phys. Chem. A* **2009**, *113*, 12763−12773.
(46) Pascher, T.; Karlsson, B. G.; Nordling, M.; Malmström, B. G.; Vänngård, T. Reduction Potentials and Their PH Dependence in Site-Directed-Mutant Forms of Azurin from Pseudomonas Aeruginosa. *Eur. J. Biochem.* **1993**, *212*, 289−296.
(47) Connick, W. B.; Di Bilio, A. J.; Hill, M. G.; Winkler, J. R.; Gray, H. B. Tricarbonyl(1,10-Phenanthroline) (Imidazole) Rhenium(I): A

https://doi.org/10.1021/acsomega.3c01589
ACS Omega 2023, 8, 19798−19806

Powerful Photooxidant for Investigations of Electron Tunneling in Proteins. *Inorg. Chim. Acta* **1995**, *240*, 169−173.
(48) Solar, S.; Getoff, N.; Surdhar, P. S.; Armstrong, D. A.; Singh, A. Oxidation of Tryptophan and N-Methylindole by N3.Cntdot., Br2.-, and (SCN)2.- Radicals in Light- and Heavy-Water Solutions: A Pulse Radiolysis Study. *J. Phys. Chem. A* **1991**, *95*, 3639−3643.
(49) Stoll, S.; Schweiger, A. EasySpin, a Comprehensive Software Package for Spectral Simulation and Analysis in EPR. *J. Magn. Reson.* **2006**, *178*, 42−55.
(50) Pettersen, E. F.; Goddard, T. D.; Huang, C. C.; Couch, G. S.; Greenblatt, D. M.; Meng, E. C.; Ferrin, T. E. UCSF Chimera—A Visualization System for Exploratory Research and Analysis. *J. Comput. Chem.* **2004**, *25*, 1605−1612.
(51) Shao, Y.; Mei, Y.; Sundholm, D.; Kaila, V. R. I. Benchmarking the Performance of Time-Dependent Density Functional Theory Methods on Biochromophores. *J. Chem. Theory Comput.* **2020**, *16*, 587−600.
(52) Winkler, J. R.; Di Bilio, A. J.; Farrow, N. A.; Richards, J. H.; Gray, H. B. Electron Tunneling in Biological Molecules. *Pure Appl. Chem.* **1999**, *71*, 1753−1764.
(53) Marcus, R. A.; Sutin, N. Electron Transfers in Chemistry and Biology. *Biochim. Biophys. Acta, Rev. Bioenerg.* **1985**, *811*, 265−322.
(54) Gray, H. B.; Winkler, J. R. Electron Tunneling through Proteins. *Q. Rev. Biophys.* **2003**, *36*, 341−372.
(55) Lakowicz, J. R. *Principles of Fluoresence Spectroscopy*, 2nd ed.; Kleuwer Academic/Plenum: New York, 1999.
(56) Fedoretz-Maxwell, B. P.; Shin, C. H.; MacNeil, G. A.; Worrall, L. J.; Park, R.; Strynadka, N. C. J.; Walsby, C. J.; Warren, J. J. The Impact of Second Coordination Sphere Methionine-Aromatic Interactions in Copper Proteins. *Inorg. Chem.* **2022**, *61*, 5563−5571.
(57) Zheng, L.; Baumann, U.; Reymond, J.-L. An Efficient One-Step Site-Directed and Site-Saturation Mutagenesis Protocol. *Nucleic Acids Res.* **2004**, *32*, No. e115.
(58) Liu, J.; Chakraborty, S.; Hosseinzadeh, P.; Yu, Y.; Tian, S.; Petrik, I.; Bhagi, A.; Lu, Y. Metalloproteins Containing Cytochrome, Iron−Sulfur, or Copper Redox Centers. *Chem. Rev.* **2014**, *114*, 4366−4469.
(59) Krzystek, J.; Sienkiewicz, A.; Pardi, L.; Brunel, L. C. DPPH as a Standard for High-Field EPR. *J. Magn. Reson.* **1997**, *125*, 207−211.
(60) Neese, F. The ORCA Program System. *Wiley Interdiscip. Rev.: Comput. Mol. Sci.* **2012**, *2*, 73−78.
(61) Neese, F. Software Update: The ORCA Program System, Version 4.0. *Wiley Interdiscip. Rev.: Comput. Mol. Sci.* **2018**, *8*, No. e1327.
(62) Neese, F. Software Update: The ORCA Program System—Version 5.0. *Wiley Interdiscip. Rev.: Comput. Mol. Sci.* **2022**, *12*, No. e1606.
(63) Neese, F.; Wennmohs, F.; Hansen, A.; Becker, U. Efficient, Approximate and Parallel Hartree−Fock and Hybrid DFT Calculations. A 'Chain-of-Spheres' Algorithm for the Hartree−Fock Exchange. *Chem. Phys.* **2009**, *356*, 98−109.
(64) Grimme, S.; Antony, J.; Ehrlich, S.; Krieg, H. A Consistent and Accurate Ab Initio Parametrization of Density Functional Dispersion Correction (DFT-D) for the 94 Elements H-Pu. *J. Chem. Phys.* **2010**, *132*, No. 154104.
(65) Grimme, S.; Ehrlich, S.; Goerigk, L. Effect of the Damping Function in Dispersion Corrected Density Functional Theory. *J. Comput. Chem.* **2011**, *32*, 1456−1465.
(66) Cossi, M.; Rega, N.; Scalmani, G.; Barone, V. Energies, Structures, and Electronic Properties of Molecules in Solution with the C-PCM Solvation Model. *J. Comput. Chem.* **2003**, *24*, 669−681.
(67) Stoychev, G. L.; Auer, A. A.; Neese, F. Automatic Generation of Auxiliary Basis Sets. *J. Chem. Theory Comput.* **2017**, *13*, 554−562.
(68) Weigend, F. Accurate Coulomb-Fitting Basis Sets for H to Rn. *Phys. Chem. Chem. Phys.* **2006**, *8*, 1057−1065.
(69) Perdew, J. P.; Ernzerhof, M.; Burke, K. Rationale for Mixing Exact Exchange with Density Functional Approximations. *J. Chem. Phys.* **1996**, *105*, 9982−9985.
(70) Adamo, C.; Barone, V. Toward Reliable Density Functional Methods without Adjustable Parameters: The PBE0 Model. *J. Chem. Phys.* **1999**, *110*, 6158−6170.

https://doi.org/10.1021/acsomega.3c01589
ACS Omega 2023, 8, 19798−19806